Research Article | Vol. 10, No. 9 / 1 September 2020 / Optical Materials Express 2321
Optical Materials EXPRESS

Chemical vapor deposition synthesized monolayer MoS_2 for Q-switching pulse generation in the 2 μm spectral region

JINGCHENG SHANG,[1] TIANLI FENG,[1,*] SHENGZHI ZHAO,[1] TAO LI,[1] JIE MA,[2,3] XIAOMIN XU,[2] NORBERT KOCH,[2,3] AND JIA ZHAO[1]

[1] School of Information Science and Engineering, Shandong University, Qingdao, 266237, China
[2] Institut für Physik & IRIS Adlershof, Humboldt-Universität zu Berlin, Newtonstrasse 15, 12489 Berlin, Germany
[3] Helmholtz-Zentrum für Materialien und Energie GmbH, 12489 Berlin, Germany
[*] tlfeng@sdu.edu.cn

Abstract: We demonstrate a monolayer MoS_2-based saturable absorber (SA) synthesized by chemical vapor deposition (CVD). The as-grown SA has high spatial homogeneity and shows excellent saturable absorption properties in the 2 μm wavelength region. A higher modulation depth of 21.3% and lower saturation intensity of 0.47 MW/cm^2 are achieved compared with those of other documented MoS_2 SAs to date. When applying the MoS_2 SA to a Tm:YAG ceramic laser, we observe a Q-switched pulse train with a shortest pulse duration of 388.0 ns under a pulse repetition rate of 82 kHz, which corresponds to a single pulse energy of 5.4 uJ and a peak power of 14 W. We believe that CVD constitutes an effective method towards high-quality MoS_2 saturable absorbers that possess remarkable application potential in the 2 μm wavelength region.

1. Introduction

Pulsed laser sources operating near 2 μm wavelength region have attracted a lot of attentions due to the numerous applications in different fields. For example, the pulsed single-frequency 2 μm laser sources have been widely used in the field of laser remote sensing for detecting the concentration of important atmospheric gases like H_2O and CO_2 in the atmospheric air. Since there exists an atmospheric window near 2 μm wavelength region, the pulsed 2 μm laser source is very suitable for wind speed detection in a Doppler LIDAR [1,2]. With a pulsed 2 μm laser sources, the emission wavelength of laser can be efficiently extended to mid-infrared wavelength region via the nonlinear frequency conversion process. The mid-infrared laser is the key to realize laser countermeasure in a combat [3]. 2 μm pulsed lasers also can be used for laser surgery due to its special blood coagulation effect which can suppress bleeding when cutting the human tissue. Meanwhile, 2 μm lasers also can be found a lot of applications in industrial material processing, biomedical imaging, et. Al. [4,5]. Therefore, a robust 2 μm pulsed laser is the basis to realize the above mentioned applications. Due to the compactness and low-cost, the passive Q-switching method based on saturable absorbers (SAs) is considered to be the most efficient way to reach such kind of laser pulses. In a passive Q-switching laser, a SA is the key to realize excellent laser performance. At present, carbon-based low dimensional materials, such as carbon nanotubes and graphene, have been employed for passive Q-switching 2 μm lasers [6–8]. However, precise control of the diameter and purity of carbon nanotubes remains a challenge, and thus a SA based on uniform carbon nanotube layers is quite difficult to realize [6]. Moreover, the carbon nanotube SA is vulnerable to the surrounding environment, making it easily deteriorated at a high temperature aerobic condition. Graphene can be grown uniformly, yet its application is limited by the inevitable oxidation in the presence of water [7]. Recently emergent two-dimensional topological insulators (TIs) hold similar advantages as the above-mentioned

#402930 https://doi.org/10.1364/OME.402930
Journal © 2020 Received 15 Jul 2020; revised 14 Aug 2020; accepted 21 Aug 2020; published 31 Aug 2020

Optical Materials EXPRESS

carbon-based materials, such as ultrafast saturation recovery time and a wide absorption band. Although TIs have shown good saturable absorption proprieties in the spectral range from 1 μm to 3 μm [9–12], their long-term properties are still influenced by the oxidation to some extent [13]. Molybdenum disulfide (MoS_2), a typical transition-metal dichalcogenide (TMD), with a hexagonal crystalline lattice, is rather stable in air and thus could provide a longer lifetime, making it suitable for solid-state lasers [14]. On the other hand, the modulation depth is an important parameter that evaluates the performance of a saturable absorber. A large modulation depth is favorable for achieving short laser pulses. MoS_2 SAs with different modulation depth have been reported in the spectral range between 1 μm and 3 μm [15–22]. A multi-layer MoS_2 SA showed a state-of-the-art modulation depth of up to 21% in the 2 μm spectral region recently [23], which is larger than the most reported values in TMDs (WS_2 or WTe_2) based SAs [24]. The large modulation depth is favorable for a short Q-switching pulse generation. For example, a previous study shows that the MoS_2 SA is superior to WS_2 in a short Q-switching pulse generation [25]. Besides, the MoS_2 SA was more efficient in the 2 μm wavelength region compared to that at 1 μm, due to a lower saturation intensity [26].

There are several methods for the preparation of MoS_2 SAs, including liquid-phase exfoliation (LPE), thermal decomposing (TD), pulsed laser deposition (PLD), vapor phase growth (VPG), and physical vapor deposition (PVD) [18,23,27]. Despite the existing techniques, fabricating a MoS_2 SA with large area, high crystallinity, as well as structural homogeneity is still challenging. With LPE, the uniformity and thickness of the MoS_2 SA cannot be precisely controlled, which often yields flakes randomly located on the substrate [23,28–30]. The other three methods, i.e., PLD, VPG, and PVD, often yield small crystalline flakes. Compared to the above-mentioned techniques, CVD possesses the advantages of low cost, high production yield, excellent scalability, as well as controllable sample quality and homogeneity [31]. In particular, the thickness of MoS_2 layers can be tuned with the growth parameters [32]. Despite the well-recognized feasibility of MoS_2 as SA for solid-state 2 μm lasers, the unique advantages of CVD-grown MoS_2, in particular, with the precisely controlled thickness and a high spatial homogeneity, have not been adequately investigated in Q-switched bulk lasers so far.

In the present contribution, we demonstrate a high-quality monolayer MoS_2 SA with good homogeneity and uniform thickness synthesized by the CVD method. The SA has a saturation intensity of 0.47 MW/cm^2, a non-saturable absorbance of 11.9%, and a modulation depth of 21.3%. The large modulation depth endows the SA with a short pulse generation ability, which eventually enables a 388 ns pulse in a 2 μm Tm:YAG ceramic laser. Compared to previous reports, the CVD grown MoS_2 SA shows unique advantages in realizing 2 μm solid-state lasers.

2. Preparation and characterization of MoS_2 SA

The employed CVD furnace for MoS_2 growth is shown in Fig. 1, in which the horizontal tube is comprised by a low temperature zone and a high temperature zone. In order to realize the sufficient mixing of Mo and S in the gas phase, the high purity Ar acts as the carrier gas, with its flow direction indicated by the arrow in Fig. 1. Before growth, flushing with the high pure Ar was performed to eliminate the residual oxygen and other contaminates inside the tube. Ultra-pure MoO_3 (~99.998%) and S (~99.98%) powder serve as the sources with their location and distance marked in Fig. 1. The sapphire substrate that hangs above the MoO_3 powders is placed in the high temperature zone. The sulphur powder kept at the low temperature zone is placed about 20 cm away from the substrate. It is known that the introduction of interfacial defects and tensile strains or stacking of several monolayers in sheets can strongly affect the band structure of MoS_2 [26]. Considering the saturable absorption of MoS_2 relies on its bandgap, so with this method we can indirectly adjust the saturable absorption properties of MoS_2. During the growing period, the thickness and defects of MoS_2 are strongly dependent on the ambient temperature inside the furnace. In the chemical reaction stage, a higher ambient temperature is beneficial to form the

Optical Materials EXPRESS

monolayer MoS_2 and a strong tensile strain, while the low ambient temperature is good for the formation of multi-layer MoS_2. Thus by simply controlling the ambient temperature one could adjust the thickness of MoS_2. But when the temperature is higher than 1050 K, the formation of MoS_2 becomes very difficult. So in the experiment, the temperature of the two zones is ramped gradually to 483 K and 1050 K. In the annealing stage, the tensile strains can be further strengthen by fast decreasing of the ambient temperature. Simultaneously, the interfacial defects also can be introduced during this fast-cooling process. So after a complete reaction of 10 mins, we use 15 sccm Ar flow for fast-cooling down. A picture of the fabricated MoS_2 on the sapphire wafer is given as the inset at the bottom right of Fig. 2(a).

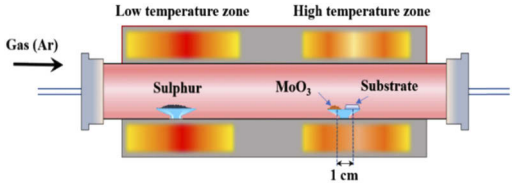

Fig. 1. Schematic diagram of the CVD furnace.

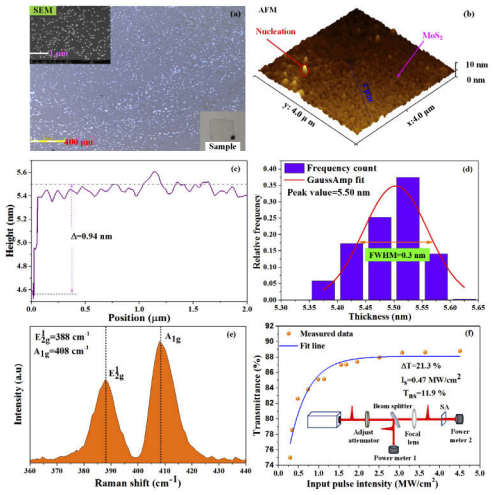

Fig. 2. (a) Optical microscopy image of the as-grown MoS_2 on sapphire. Scale bar: 400 μm. Inset: as-grown MoS_2 covering the whole sapphire wafer (the bottom right) and the scanning electron microscope (SEM) image (the top left). (b) AFM topographic image of the same sample in (a) with a dimension of 4 μm×4 μm×10 nm. (c) The height profile of MoS_2 over a length of 2 μm. (d) The thickness distribution of the MoS_2 film. (e) Raman spectrum of the CVD synthesized MoS_2. (f) The nonlinear transmission of the fabricated MoS_2 SA. Inset: the experimental setup for nonlinear transmission measurement.

In order to evaluate the homogeneity of the CVD fabricated MoS_2, we take an optical microscope (OM) image, a scanning electron microscope (SEM) image, and an atomic force microscope (AFM) image respectively, which are shown as Fig. 2(a) and Fig. 2(b). The bright spot in Fig. 2(a) indicates the original nucleation sites, and the gray area is mainly the synthetic MoS_2. The monolayer MoS_2 covers about 80% space of the sapphire substrate, while the rest part is dominated by multi-layered MoS_2, distributing randomly on the substrate. Figure 2(b) is the AFM image with a scanning size of area of 4 μm×4 μm, which indicates the height of the MoS_2 film is around 0.94 nm [see Fig. 2(c)] with a slight fluctuation of about 0.15 nm [see Fig. 2(d)].

Optical Materials EXPRESS

Considering the single layer MoS_2 has a thickness of 0.65 nm [31], the synthesized film has a monolayer structure. The monolayer structure is further verified by the measured Raman spectrum in Fig. 2(e), which has two characteristic peaks (in-plane mode E^1_{2g} and out-of-plane mode A_{1g} [32]) with a separation of 20 cm^{-1}. The measured small-signal transmission of the monolayer MoS_2 around 2 μm approaches to 91%, which is close to the reported values [20,26,29]. To obtain the saturable absorption characteristics of the monolayer MoS_2 at 2μm, its nonlinear transmission is measured by a pair of balanced twin-detectors [33] [inset figure of Fig. 2(f)]. The pump source is a Tm:YAG laser with a center wavelength of 1985nm and pulse duration of 200 ns. The obtained data is theoretically fitted with the following equation [Fig. 2(f)]:

$$T(I) = 1 - \Delta T exp\left(-\frac{I}{I_{sat}}\right) - T_{ns}. \quad (1)$$

Where ΔT and T_{ns} are the modulation depth and non-saturable absorption of SA, respectively. I and I_{sat} are the pulse intensity and saturation intensity of the input pulse, respectively. Based on the fitted result, the modulation depth of 21.3%, saturation intensity of 0.47 MW/cm^2 and non-saturable absorption of 11.9% are determined.

For a parallel comparison, we summarize the saturable absorption characteristics of MoS_2 SA fabricated by different methods at 2 μm in Fig. 3. The x-axis in Fig. 3 is modulation depth, while the y-axis are saturation intensity and non-saturable absorption respectively. From Fig. 3(a), it can be found that the CVD synthesized MoS_2 SA has the lowest saturation intensity of 0.47 MW/cm^2, which is slight lower than that of graphene (about 0.6 MW/cm^2) [26]. Meanwhile, the CVD synthesized MoS_2 SA has the state-of-art modulation depth and a moderate non-saturable absorption loss [see Fig. 3(b)]. Despite a very high purity and homogeneity, the CVD synthesized MoS_2 still has a high non-saturable absorption losses of 11.9%, which is not superior to the previous reported results. We attribute this to the scattering induced by the nucleation and the sapphire substrate. The saturable absorption characters of the CVD synthesized MoS_2 SA are quite similar with that reported in Ref. [23], in which the SA is synthesized by LPE method. But the SA reported in that work has a bad uniformity, which shows a large thickness variation about 2 nm. Furthermore, due to the roughness surface and non-uniform thickness of the MoS_2 SA, the LPE method fabricated MoS_2 SAs exhibit a huge difference between each other. In comparison, these disadvantages rarely occur in the CVD fabricated MoS_2 SAs, which with a good characterization result as shown above.

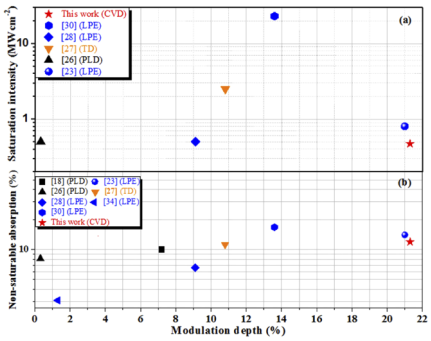

Fig. 3. The saturable absorption characteristics of MoS_2 SA fabricated with different methods in the 2 μm wavelength region. Different color indicates different fabrication method. X-axis indicates the modulation depth and Y-axis gives the saturation intensity in Fig. 3(a) and the non-saturable absorption in Fig. 3(b).

Optical Materials EXPRESS

3. Experiment setup and discussion

We further investigate the saturable absorption properties of the CVD synthesized MoS_2 SA at 2 μm wavelength region by applying it to a passive Q-switching Tm:YAG ceramic laser system (Fig. 4). A 3 mm×3 mm×6 mm Tm: YAG (5 at. %) ceramic with the advantages of stable chemical properties, ease of fabrication, and capable of high concentration doping is selected as the gain medium. The pump light is coupled out through an optical fiber from a 793 nm laser diode (LD), then focused into the Tm: YAG ceramic with a 1:1 telescope. In order to effectively remove the generated heat, the gain medium is water-cooled at 13 °C by a cooling system. The laser cavity is built with two plan mirrors (M_1 and M_2) with a total length of 3.5 cm. The input plan mirror M_1 is highly reflective (HR) coated from 1820 nm to 2150 nm (reflectivity > 99.9%) and anti-reflection (AR) coated around 790 nm. The plan mirror M_2 with a transmittance of 3% from 1820 nm to 2150 nm acts as an output coupler. After M_2, a filter is employed to block the pump laser. The Q-switching pulse profile is detected by an InGaAs PIN detector (EOT, ET-5000) and observed with an oscilloscope (Tektronix, DPO 4102B-L). The average output power is measured with a laser power meter (CNI, TS35).

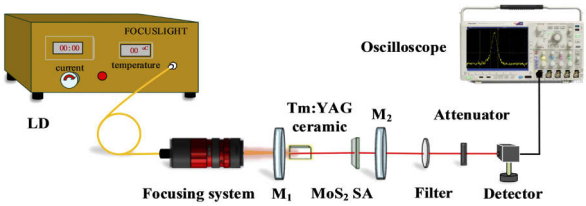

Fig. 4. Schematic configuration of the passively Q-switched Tm:YAG ceramic laser.

The power performances of the continuous-wave (cw) and passive Q-switching (PQS) laser are shown in Fig. 5(a). The maximum absorbed pump power is limited within 8.3 W for getting a stable Q-switching operation. The thresholds for cw and PQS are both close to the absorbed pump power of 2 W. The slight threshold difference arises from the small saturated intensity of the monolayer MoS_2 SA and the low intracavity loss induced by the flat surface of MoS_2 SA. The slope efficiencies of 10.4% and 7.0% are achieved for cw and PQS regimes respectively. The maximum output powers of 660 mW is obtained in cw regime, corresponding to a power instability of 1.8% measured within 60 min. The introduced MoS_2 SA deteriorates the laser output, resulting in a maximum output power of 445 mW with a power instability of 6.2% under the same absorbed pump power. The emission wavelength of the Tm:YAG laser is measured by employing a NIR spectrometer (Avaspec, NIR256-2.5TEC) with a resolution of 7 nm [Fig. 5(b)]. In the cw regime, single wavelength radiation at 2015 nm with a full width at half maximum (FWHM) of 16.8 nm is achieved [inset figure of Fig. 5(b)]. Despite the low resolution of the spectrometer, we still observe a stable dual-wavelength operation at 1996nm and 2027nm in the PQS regime. We believe the dual-wavelength emission is induced by the etalon effect from the substrate of the MoS_2 SA.

The beam quality factors (M^2 factors) shown in Fig. 6(a) in PQS regime are measured by using the 90.0/10.0 scanning-knife edge method at the maximum average output power. The determined M^2 factors from the fitted curve are 1.27 and 1.22 in tangential and sagittal direction respectively. These values are slight larger than the ideal values of 1 in each direction, which arise from the thermal lens effect of gain medium and the slight mode mismatching between pumping beam (105 μm) and intracavity mode (120 μm).

Figure 6(b) shows the pulse profile at the maximum average output power of 445 mW. A shortest pulse duration of 388 ns is obtained at a pulse repetition rate of 82 kHz. Considering the Q-switching pulse still exists stably at the maximum average output power of 445 mW, we

Optical Materials EXPRESS

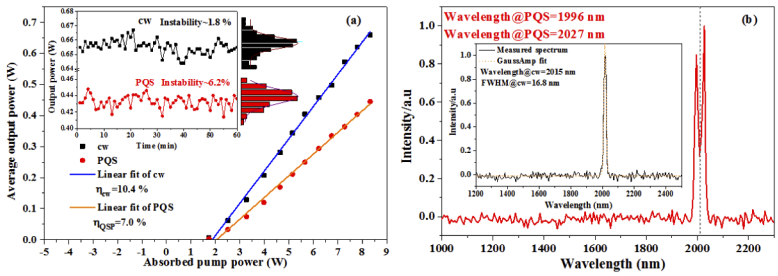

Fig. 5. (a) The power performance in cw and PQS regimes (inset: the statistical distributions of maximum output power for 60 mins). (b) The emission spectra in cw (inset figure) and PQS regimes.

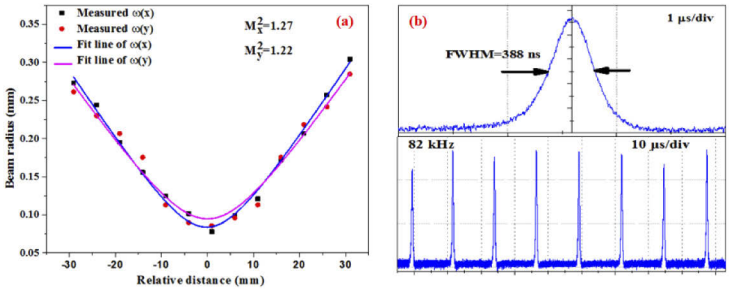

Fig. 6. (a) M^2 factors in tangential and sagittal direction. (b) The pulse profile and the pulse train at the maximum absorbed pump power in Q-switching regime with MoS_2 SA.

estimate the damage threshold of MoS_2 is higher than 1.5 MW/cm^2. Figure 7(a) gives the pulse durations and repetition rates at different absorbed pump power. Due to the increasing intracavity photon intensity, the bleaching time of the SA is shortened, resulting in a decreasing of the pulse duration from 1325 ns to 388 ns and an increasing of the pulse repetition rate from 39 to 82 kHz. For a passive Q-switching laser pulse, further shorten the Q-switching pulse duration could be achieved by decreasing the cavity length and improving the modulation depth of SA according to the Ref. [35]. For example, a much shorter pulse duration of 175 ns is achieved in a 2 μm microchip laser which only has a cavity length of 4 mm [26]. Figure 7(b) shows the single pulse energy and pulse peak power versus the absorbed pump power. The maximum single pulse energy of 5.4 μJ is achieved at the absorbed pump power of 8.3 W, corresponding to a peak power of 14 W.

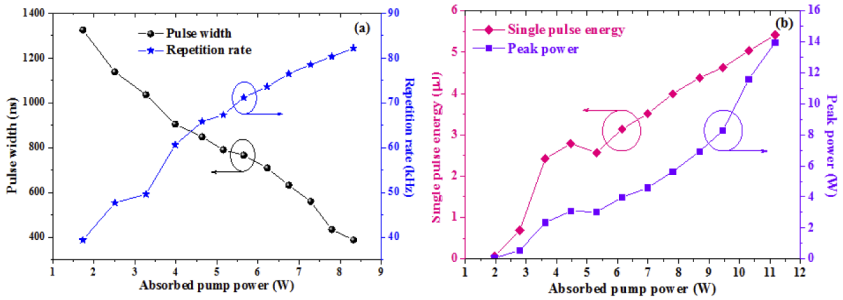

Fig. 7. (a) The pulse duration and repetition rate versus the absorbed pump power. (b) The single pulse energy and pulse peak power versus absorbed pump power.

Optical Materials EXPRESS

The reported MoS_2 passive Q-switching properties in the 2 μm bulk laser is summarized in Table 1. The pulse duration of 388 ns is only slightly larger than the Q-switching microchip laser reported in Ref. [26]. However, we find that the modulation depth (0.32%) of the MoS_2 fabricated by PLD in Ref. [26] is much smaller than our case. So we believe the pulse duration in the microchip laser could be further shortened with a CVD prepared MoS_2 SA. Meanwhile, the pulse duration of 388 ns is shorter than that obtained from other low dimensional materials (WS_2, Black phosphorus, WSe_2, BN, Graphene oxide, Gold nanorods, $SnSe_2$, Single-walled carbon nanotubes, and Graphene) summarized in Ref. [33]. The maximum output power of 445 mW, single pulse energy of 5.4 μJ and peak power of 14 W are also larger than most of the reported values in Table 1. Above analyses could demonstrate the monolayer MoS_2 SA is more suitable for short Q-switching laser pulse generation with high pulse energy in 2 μm wavelength region. Moreover, the CVD method is reliable to obtain such high quality monolayer MoS_2.

Table 1. Comparison of passive Q-switching 2 μm solid-state lasers based on MoS_2 SA.

Ref	Fabricated method for MoS_2 SA	T_{OC}	Shortest pulse duration	Highest repetition rate	Maximum output power	Maximum Single pulse energy	Maximum peak power
		%	ns	kHz	mW	μJ	W
[18]	PLD	2	4840	110	62	0.72	0.15
[20]	PLD	5	410	149	206	1.38	3.4
[23]	LPE	2	497	81	399	4.9	9.9
		5	435	55	270	4.9	11.3
[26]	PLD	5	175	170.0	1270	7.5	42.8
[28]	LPE	2	458.8	83.1	410	4.9	10.7
[34]	LPE	5	616	73.0	3100	42.5	68.7
[36]	TD	2	800	48.1	304	2.1	2.6
[37]	LPE	5	2610	133.6	550	4.2	1.6
		7	1640	110.0	688	6.3	3.8
		10	2370	133.2	3300	24.8	10.5
This work	CVD	3	388	82	445	5.4	14

4. Conclusion

In this work, a monolayer MoS_2 SA is fabricated by CVD and its saturable absorption properties are characterized in the 2 μm spectral region. The CVD prepared MoS_2 has a good homogeneity and uniform thickness. A large modulation depth of 21.3% and a low saturation intensity of 0.47 MW/cm^{-2} are demonstrated, which has not been reported before for MoS_2 SAs. Using the MoS_2 SA, a passively Q-switched Tm:YAG ceramic laser with multi-wavelength emission around 2 μm is realized. The obtained output characteristics, *i.e.*, 388 ns pulse duration, 5.4 μJ single pulse energy and 14 W peak power, are better than most of the previously reported results. We believe the CVD fabricated MoS_2 SA with the advantage of large area, excellent crystalline quality and homogeneity is highly suitable for 2 μm pulse laser generation.

Funding

Qilu Young Scholar Program of Shandong University; Taishan Scholar Foundation of Shandong Province (tsqn201812010); Deutsche Forschungsgemeinschaft (182087777 - SFB 951); Natural Science Foundation of Shandong Province (ZR2018MF033); National Natural Science Foundation of China (61775119).

Optical Materials EXPRESS

Disclosures

The authors declare no conflicts of interest.

References

1. S. W. Henderson, P. J. M. Suni, C. P. Hale, S. M. Hannon, J. R. Magee, D. L. Bruns, and E. H. Yuen, "Coherent laser radar at 2 μm using solid-state lasers," IEEE Trans. Geosci. Remote Sensing **31**(1), 4–15 (1993).
2. G. J. Koch, J. Y. Beyon, B. W. Barnes, M. Petro, J. Yu, F. Amzajerdian, M. J. Kavaya, and U. N. Singh, "High energy 2 μm Doppler lidar for wind measurements," Opt. Eng. **46**(11), 116201 (2007).
3. S. Chandra, M. E. Wager, B. Clayton, A. G. Geiser, T. H. Allik, J. L. Ahl, C. R. Miller, P. A. Budni, P. A. Ketteridge, K. G. Lanier, E. P. Chicklis, J. A. Hutchinson, and W. W. Hovis, "2 μm-pumped 8-12 μm OPO source for remote chemical sensing," Proc. SPIE **4036**, 200–208 (2000).
4. W. M. Steen and J. Mazumder, "Laser Bending or Forming," in *Laser Material Processing*, 4th Edition (Springer Verlag Publishing, 2010), pp. 301–325.
5. H. Lubatschowski and A. Heisterkamp, "Ophthalmic Applications," in *Femtosecond Technology for Technical and Medical Applications*, TAP, 96 (Springer Verlag Publishing, 2004), pp. 187–203.
6. P. Avouris, M. Freitag, and V. Perebeinos, "Carbon-nanotube photonics and optoelectronics," Nat. Photonics **2**(6), 341–350 (2008).
7. H. T. Zhu, L. N. Zhao, J. Liu, S. C. Xu, W. Cai, S. Z. Jiang, L. H. Zheng, L. B. Su, and J. Xu, "Monolayer graphene saturable absorber with sandwich structure for ultrafast solid-state laser," Opt. Eng. **55**(8), 081304 (2016).
8. A. S. Yasukevich, P. Loiko, N. V. Gusakova, J. M. Serres, X. Mateos, K. V. Yumashev, N. V. Kuleshov, V. Petrov, U. Griebner, M. Aguiló, and F. Díaz, "Modelling of graphene Q-switched Tm lasers," Opt. Commun. **389**(15), 15–22 (2017).
9. H. Zhang, C. Liu, X. Qi, X. Dai, Z. Fang, and S. Zhang, "Topological insulators in Bi_2Se_3, Bi_2Te_3 and Sb_2Te_3 with a single Dirac cone on the surface," Nat. Phys. **5**(6), 438–442 (2009).
10. Z. Luo, Y. Huang, J. Weng, H. Cheng, Z. Lin, B. Xu, Z. Cai, and H. Xu, "1.06 μm Q-switched ytterbium-doped fiber laser using few-layer topological insulator Bi_2Se_3 as a saturable absorber," Opt. Express **21**(24), 29516–29522 (2013).
11. J. Qiao, S. Zhao, K. Yang, W. Song, W. Qiao, C. Wu, J. Zhao, G. Li, D. Li, H. Liu, and C. Lee, "High-quality 2-μm Q-switched pulsed solid-state lasers using spin-coating-coreduction approach synthesized Bi_2Te_3 topological insulators," Photonics Res. **6**(4), 314–320 (2018).
12. R. Miao, M. Tong, K. Yin, H. Ouyang, Z. Wang, X. Zheng, X. Cheng, and T. Jiang, "Soliton mode-locked fiber laser with high-quality MBE-grown Bi_2Se_3 film," Chin. Opt. Lett. **17**(7), 071403 (2019).
13. L. V. Yashina, J. Sánchez-Barriga, M. R. Scholz, A. A. Volykhov, A. P. Sirotina, V. Neudachina, M. Tamm, A. Varykhalov, D. Marchenko, G. Springholz, G. Bauer, A. Knop-Gericke, and O. Rader, "Negligible surface reactivity of topological insulators Bi_2Se_3 and Bi_2Te_3 towards oxygen and water," ACS Nano **7**(6), 5181–5191 (2013).
14. H. Sener Sen, H. Sahin, F. M. Peeters, and E. Durgun, "Monolayers of MoS_2 as an oxidation protective nanocoating material," J. Appl. Phys. **116**(8), 083508 (2014).
15. K. Wang, J. Wang, J. Fan, M. Lotya, A. O'Neill, D. Fox, Y. Feng, X. Zhang, B. Jiang, Q. Zhao, H. Zhang, J. N. Coleman, L. Zhang, and W. J. Blau, "Ultrafast saturable absorption of two-dimensional MoS_2 nanosheets," ACS Nano **7**(10), 9260–9267 (2013).
16. H. Zhang, S. B. Lu, J. Zheng, J. Du, S. C. Wen, D. Y. Tang, and K. P. Loh, "Molybdenum disulfide (MoS_2) as a broadband saturable absorber for ultra-fast photonics," Opt. Express **22**(6), 7249 (2014).
17. B. Xu, Y. J. Cheng, Y. Wang, Y. Z. Huang, J. Peng, Z. Q. Luo, H. Y. Xu, Z. P. Cai, J. Weng, and R. Moncorgé, "Passively Q-switched Nd:$YAlO_3$ nanosecond laser using MoS_2 as saturable absorber," Opt. Express **22**(23), 28934 (2014).
18. L. C. Kong, G. Q. Xie, P. Yuan, L. J. Qian, S. X. Wang, H. H. Yu, and H. J. Zhang, "Passive Q-switching and Q-switched mode-locking operations of 2 μm Tm:CLNGG laser with MoS_2 saturable absorber mirror," Photonics Res. **3**(2), A47 (2015).
19. C. Wang, S. Z. Zhao, T. Li, K. J. Yang, C. Luan, X. D. Xu, and J. Xu, "Passively Q-switched Nd:LuAG laser using few-layered MoS_2 as saturable absorber," Opt. Commun. **406**(1), 249–253 (2018).
20. S. Wang, H. Yu, H. Zhang, A. Wang, M. Zhao, Y. Chen, L. Mei, and J. Wang, "Broadband few-layer MoS_2 saturable absorber," Adv. Mater. **26**(21), 3538–3544 (2014).
21. M. Q. Fan, T. Li, S. Z. Zhao, G. Q. Li, H. Y. Ma, X. C. Gao, C. Krankel, and G. Huber, "Watt-level passively Q-switched Er:Lu_2O_3 laser at 2.84 μm using MoS_2," Opt. Lett. **41**(3), 540 (2016).
22. K. Wang, K. Yang, X. Zhang, S. Zhao, C. Luan, C. Liu, J. Wang, X. Xu, and J. Xu, "passively Q-switched laser at 1.3 μm with few-layered MoS_2 saturable absorber," IEEE J. Sel. Top. Quantum Electron. **23**(1), 71 (2017).
23. C. Luan, X. Zhang, J. Zhao, S. Zhao, K. Yang, T. Li, W. Qiao, H. Chu, J. Qiao, J. Wang, L. Zheng, X. Xu, and J. Xu, "High-peak power passively Q-switched 2 μm laser with MoS_2 saturable absorber," IEEE J. Sel. Top. Quantum Electron. **23**(1), 66–70 (2017).
24. B. Chen, X. Zhang, K. Wu, H. Wang, J. Wang, and J. Chen, "Q-switched fiber laser based on transition metal dichalcogenides MoS_2, $MoSe_2$, WS_2, and WSe_2," Opt. Express **23**(20), 26723–26737 (2015).

Optical Materials EXPRESS

25. G. Zhao, S. Han, A. Wang, Y. Wu, M. Zhao, Z. Wang, and X. Hao, ""Chemical Weathering" Exfoliation of Atom-Thick Transition Metal Dichalcogenides and Their Ultrafast Saturable Absorption Properties," Adv. Funct. Mater. **25**(33), 5292–5299 (2015).
26. J. M. Serres, P. Loiko, X. Mateos, H. Yu, H. Zhang, Y. Chen, V. Petrov, U. Griebner, K. Yumashev, M. Aguilo, and F. Diaz, "MoS_2 saturable absorber for passive Q-switching of Yb and Tm microchip lasers," Opt. Mater. Express **6**(10), 3262–3273 (2016).
27. C. Zhang, P. Ge, X. Fan, J. Liu, S. Jiang, Y. Xu, and B. Man, "MoS_2 saturable absorber for a Q-switched mode-locked 2 μm laser," Laser Phys. **29**(1), 015803 (2019).
28. Z. Niu, K. Yang, T. Li, J. Zhao, S. Zhao, G. Li, D. Li, W. Qiao, H. Chu, K. Gao, and X. Liu, "Doubly passively Q-switched Tm:YAP laser with MoS_2 and WS_2 saturable absorbers at 2 μm," Optik **198**, 163205 (2019).
29. Z. Luo, Y. Huang, M. Zhong, Y. Li, J. Wu, B. Xu, H. Xu, Z. Kai, J. Peng, and J. Weng, "1-, 1.5-, and 2-μm Fiber Lasers Q-Switched by a Broadband Few-Layer MoS_2 Saturable Absorber," J. Lightwave Technol. **32**(24), 4679–4686 (2014).
30. Z. Tian, K. Wu, L. Kong, N. Yang, Y. Wang, R. Chen, W. Hu, J. Xu, and Y. Tang, "Mode-locked thulium fiber laser with MoS_2," Laser Phys. Lett. **12**(6), 065104 (2015).
31. P. Gnanasekar, D. Periyanagounder, A. Nallathambi, S. Subramani, M. Palanisamy, and J. Kulandaivel, "Promoter free synthesis of monolayer MoS_2 by chemical vapour deposition," CrystEngComm **30**(2), 1–8 (2018).
32. F. Chen, W. Su, S. Ding, and L. Fu, "Growth and optical properties of large-scale MoS_2 films with different thickness," Ceram. Int. **45**(12), 15091–15096 (2019).
33. J. Shang, T. Feng, S. Zhao, T. Li, Z. Pan, and J. Zhao, "Saturable absorption characteristics of Bi_2Se_3 in a 2 μm Q-switching bulk laser," Opt. Express **28**(4), 5639–5647 (2020).
34. Y. Xue, Z. Xie, Z. Ye, X. Hu, J. Xu, and H. Zhang, "Enhanced saturable absorption of MoS_2 black phosphorus composite in 2 μm passively Q-switched Tm: YAP laser," Chin. Opt. Lett. **16**(2), 020018 (2018).
35. G. J. Spühler, R. Paschotta, R. Fluck, B. Braun, M. Moser, G. Zhang, E. Gini, and U. J. Keller, "Experimentally confirmed design guidelines for passively Q-switched microchip lasers using semiconductor saturable absorbers," J. Opt. Soc. Am. B **16**(3), 376–388 (1999).
36. P. G. Ge, J. Liu, S. Z. Jiang, Y. Y. Xu, and B. Y. Man, "Compact Q-switched 2 μm Tm:$GdVO_4$ laser with MoS_2 absorber," Photonics Res. **3**(5), 256 (2015).
37. G. Li, X. Yang, and L. Zhou, "A 3.3-W passive Q-switched 2-μm laser with a MoS_2-based saturable absorber," IOP Conf. Ser.: Earth Environ. Sci. **242**, 032001 (2019).